

# Symmetric Chaos in a Local Codimension Two Bifurcation with the Symmetry Group of a Square

Stella Abreu <sup>\*</sup>      Philip Aston <sup>†</sup>      Ian Melbourne <sup>‡</sup>

9 January, 2004

## Abstract

We study a codimension two steady-state/steady-state mode interaction with  $\mathbb{D}_4$  symmetry, where the centre manifold is three-dimensional. Primary branches of equilibria undergo secondary Hopf bifurcation to periodic solutions which undergo tertiary bifurcations leading to chaotic dynamics. This is not an exponentially small effect, and the chaos obtained in simulations using DsTool is large-scale, in contrast to the ‘weak’ chaos associated with Shilnikov theory.

Moreover, there is an abundance of *symmetric chaotic attractors* and *symmetry-increasing bifurcations*. Numerical investigations demonstrate that the symmetric chaos is part of the local codimension two bifurcation. The two-dimensional parameter space is mapped out in detail for a specific choice of Taylor coefficients for the centre manifold vector field. We use AUTO to compute the transitions involving periodic solutions, Lyapunov exponents to determine the chaotic region, and symmetry detectives to determine the symmetries of the various attractors.

**Keywords:** Symmetric chaos, symmetry-increasing bifurcations, local bifurcation theory, mode interaction.

**AMS classification numbers:** 37G40, 37G30, 34C28

---

<sup>\*</sup>Departamento de Matemática, Universidade Portucalense, R. António Bernardino de Almeida, 541/619, 4200 Porto, Portugal

<sup>†</sup>Department of Maths and Stats, University of Surrey, Guildford GU2 7XH, UK

<sup>‡</sup>Department of Maths and Stats, University of Surrey, Guildford GU2 7XH, UK

# 1 Introduction

In dynamical systems with symmetry, it is possible to obtain chaotic attractors with *symmetry on average*, where the symmetry of the attractor as a set is greater than the symmetry of the individual points in the attractor. Such *symmetric attractors* were studied by Chossat & Golubitsky [7] who also identified a mechanism called *symmetry-increasing bifurcation* where distinct but symmetrically related chaotic attractors collide to produce an attractor with greater symmetry. (This is related to the notion of *crises* [17].) Subsequent work on numerical and theoretical aspects of symmetric attractors includes [21, 9, 23, 2, 11, 14, 20].

Hitherto, the notions of symmetric chaos and symmetry increasing bifurcation have been seen as part of global, rather than local, bifurcation theory. In this paper, we show that a variety of symmetry increasing bifurcations between chaotic attractors occur in an (at first sight, simple) example in low-codimension, low-dimensional bifurcation theory. In contrast to codimension two bifurcations for nonsymmetric vector fields [18, Chapter 7], the chaotic dynamics is determined at finite order in the Taylor series of the vector field. (For alternative examples of low-codimension bifurcations with chaotic dynamics determined at finite order, we refer to [1, 19, 13, 24, 8].)

Specifically, we study a codimension two bifurcation with  $\mathbb{D}_4$  symmetry. The bifurcation is a steady-state/steady-state mode interaction where two independent families of real eigenvalues pass simultaneously through zero. One family of eigenvalues is simple, and the other has multiplicity two corresponding to the standard representation of  $\mathbb{D}_4$ . Hence, centre manifold reduction leads to a three-dimensional vector field.

In the mode-interaction that we study, the action of  $\mathbb{D}_4$  on the centre manifold  $\mathbb{R}^3$  is defined by

$$\rho : (x, y, w) \mapsto (-y, x, w), \quad \kappa : (x, y, w) \mapsto (x, -y, -w).$$

Thus  $(x, y)$  transforms under the standard action of  $\mathbb{D}_4$ , while rotations act trivially on  $w$ . It follows from standard arguments that there are three primary branches of equilibria with maximal isotropy which we label  $\mathbb{Z}_4$ ,  $\mathbb{D}_1^e$  and  $\mathbb{D}_1^v$ . (These are cyclic subgroups generated by  $\rho$ ,  $\kappa$  and  $\kappa\rho$  respectively. The superscripts  $e$  and  $v$  stand for ‘edge’ and ‘vertex’, distinguishing the two different types of reflection symmetry of a square — axes through opposite edges and axes through opposite vertices.)

In a mode-interaction, the primary branches may undergo secondary bifurcations to branches of *mixed-mode* solutions. It turns out that all three of the primary branches above may undergo secondary Hopf bifurcations leading to periodic solutions with trivial spatial isotropy and nontrivial spatiotemporal symmetry.

In the sequel, we disregard the  $\mathbb{D}_1^v$  branch, and focus on secondary bifurcations from the  $\mathbb{Z}_4$  and  $\mathbb{D}_1^e$  branches. There is a scenario where both the  $\mathbb{Z}_4$  and  $\mathbb{D}_1^e$  branches

lose stability to supercritical Hopf bifurcations. The resulting periodic solutions have  $\frac{1}{4}$  and  $\frac{1}{2}$  phase shift symmetries respectively. Since these periodic solutions have different phase-shift symmetry, they cannot coalesce and further tertiary bifurcations are required if the branches are to connect.

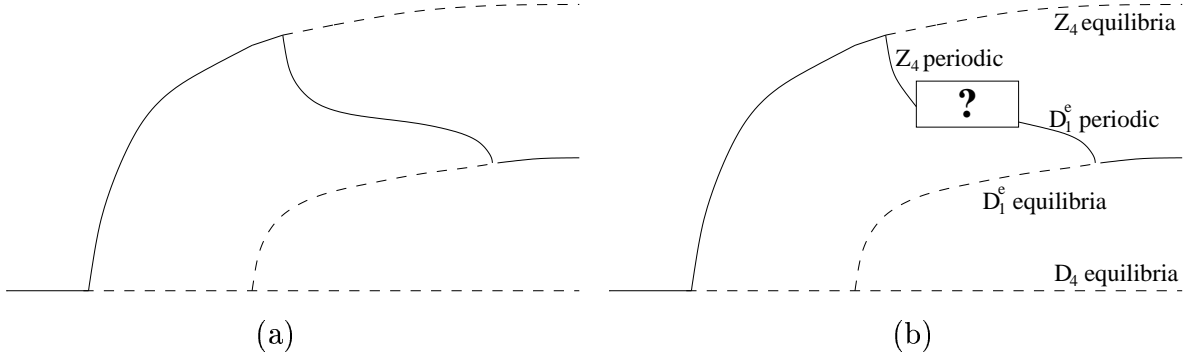


Figure 1: Schematic bifurcation diagrams for mode-interactions in steady-state/steady-state bifurcations with (a)  $\mathbb{Z}_2 \times \mathbb{Z}_2$  symmetry, and (b)  $\mathbb{D}_4$  symmetry. Solid lines denote asymptotically stable solutions and dashed lines denote unstable solutions.

The situation up to this point is summarised in Figure 1. In Figure 1(a), we show the “classical” bifurcation diagram for codimension two mode interactions, where there are nonhysteretic transitions between two primary branches of “pure mode” solutions via a secondary branch of “mixed mode” solutions. This particular diagram occurs in a steady-state/steady-state bifurcation with  $\mathbb{Z}_2 \times \mathbb{Z}_2$  symmetry [15, Figure 4.3(c), Chapter X]. (All branches here consist of equilibria and, in the usual way, solid lines denote asymptotically stable solutions and dashed lines denote unstable solutions.)

In contrast, Figure 1(b) shows the bifurcation diagram for the steady-state/steady-state bifurcation with  $\mathbb{D}_4$  symmetry studied in this paper. The mixed-mode branches now consist of periodic solutions, but more significantly their spatiotemporal symmetries are different, and so the bifurcation diagram cannot be complete.

Surprisingly, we find that the missing portion of the bifurcation diagram in Figure 1(b) takes the form of symmetric chaos. Indeed, we compute the existence of attractors with symmetry on average  $\mathbb{D}_1^o$  and  $\mathbb{D}_4$ , as well as asymmetric chaotic attractors, and we compute transitions between these different types of chaotic attractor. (We also find chaotic attractors with symmetry  $\mathbb{D}_1^e$  and  $\mathbb{D}_2^e$ , but we do not focus on these here.)

As far as we know, this is the simplest situation in local bifurcation theory for which symmetry-increasing bifurcations have been documented. We note however

that symmetric chaos has been previously seen in  $\mathbb{D}_4$ -symmetric Takens-Bogdanov bifurcations (codimension two bifurcation, four-dimensional centre manifold) [1, 25]. Armbruster *et al.* [1] found a ‘weakly chaotic’ symmetric attractor, though the symmetry was not mentioned explicitly. In the same situation, Rucklidge [25] made an extensive study of symmetric chaos and symmetry-increasing bifurcations, though the analysis was restricted to parameters near to an  $\mathbf{O}(2)$ -symmetric limit, so the effective codimension is three.

The mode-interaction that we study has been partially analysed in previous work of Lari-Lavassani *et al.* [22, Section 4.2], In particular, [22] pointed out that the existence of secondary periodic solutions bifurcating from the  $\mathbb{Z}_4$  equilibria should be expected on representation-theoretic grounds. There are no general principles that predict the nature of secondary bifurcations from the remaining primary branches, but concrete calculations show that both secondary steady-state and Hopf bifurcations can occur depending on the details of the bifurcation problem. These bifurcations and the existence of symmetric chaos and symmetry-increasing bifurcations were not studied in [22].

Our study is a combination of analytic and numerical computations. The analytic computations, which suffice for the primary and secondary bifurcations, are carried out in Section 2. Tertiary bifurcations are analysed using AUTO [12] and DsTool [3] in Section 3. In Sections 4 and 5, the existence of symmetric chaotic attractors is established by computing Lyapunov exponents and symmetry detectives [4, 10]. In Section 6, we summarise our results and describe possible future directions.

## 2 Primary and secondary bifurcations

We begin by writing down the general form of the vector field on the centre manifold.

**Proposition 2.1** *The general smooth  $\mathbb{D}_4$ -equivariant mapping  $f : \mathbb{R}^3 \rightarrow \mathbb{R}^3$  has the form*

$$\begin{aligned} f_1(x, y, w) &= h_1(x^2, y^2, w^2)x - h_2(x^2, y^2, w^2)wy \\ f_2(x, y, w) &= h_1(y^2, x^2, w^2)y + h_2(y^2, x^2, w^2)wx \\ f_3(x, y, w) &= h_3(x^2 + y^2, x^2y^2, w^2)w + h_4(x^2 + y^2, x^2y^2, w^2)xy(x^2 - y^2) \end{aligned}$$

where  $h_1, h_2, h_3, h_4$  are smooth real-valued functions.

**Proof** This is standard, as in [16]. ■

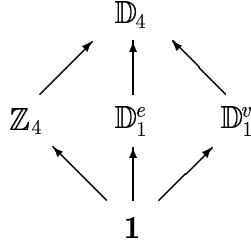
In this paper, we consider the truncated vector field

$$\left. \begin{aligned} \dot{x} &= (\lambda - x^2 + by^2 + dw^2)x - wy \\ \dot{y} &= (\lambda - y^2 + bx^2 + dw^2)y + wx \\ \dot{w} &= (\mu + c(x^2 + y^2) - w^2)w + exy(x^2 - y^2) \end{aligned} \right\} \quad (2.1)$$

In the usual way, certain (generically nonzero) coefficients can be normalised to  $\pm 1$  and we have chosen  $-1$  to ensure that certain primary branches are supercritical.

**Remark 2.2** For computations of equilibria, it is possible to use singularity theory to find a suitable truncation of these equations. Recent techniques [6] make the application of singularity theory more tractable. For our situation, a computation [5] shows that the bifurcating equilibria are determined by the vector field (2.1) with  $d = e = 0$ . However, this leads to degenerate secondary Hopf bifurcations, necessitating nonzero values for  $d$  and  $e$ .

**Isotropy subgroups** The isotropy subgroups are given up to conjugacy by  $\mathbb{D}_4$ ,  $\mathbb{Z}_4$ ,  $\mathbb{D}_1^e$ ,  $\mathbb{D}_1^v$  and  $\mathbf{1}$ , with the following lattice of inclusions:



The proper isotropy subgroups  $\mathbb{Z}_4$ ,  $\mathbb{D}_1^e$  and  $\mathbb{D}_1^v$  have one-dimensional fixed-point subspaces:

$$\text{Fix } \mathbb{Z}_4 = \{(0, 0, w)\}, \quad \text{Fix } \mathbb{D}_1^e = \{(x, 0, 0)\} \quad \text{Fix } \mathbb{D}_1^v = \{(x, x, 0)\}.$$

## Primary bifurcations

Table 1 lists the three primary branches of equilibria, showing the branching equations and the eigenvalues for the equilibria.

**Proposition 2.3** *The  $\mathbb{Z}_4$  equilibria exist for  $\mu > 0$ . They are asymptotically stable if  $\lambda + d\mu < 0$  and unstable if  $\lambda + d\mu > 0$ .*

*The  $\mathbb{D}_1^e$  equilibria exist for  $\lambda > 0$ . They are asymptotically stable if*

$$\mu + (1 + b + c)\lambda < 0, \quad (1 + b)\mu + ((1 + b)c - e)\lambda > 0,$$

Isotropy $\Sigma$	Fix $\Sigma$	Branching equation	Eigenvalues
$\mathbb{Z}_4$	$(0, 0, w)$	$\mu = w^2$	$-2\mu, \lambda + d\mu \pm i\sqrt{\mu}$
$\mathbb{D}_1^e$	$(x, 0, 0)$	$\lambda = x^2$	$-2\lambda$ , eigenvalues of $2 \times 2$ matrix with tr = $\mu + (1 + b + c)\lambda$ det = $\lambda\{(1 + b)\mu + ((1 + b)c - e)\lambda\}$
$\mathbb{D}_1^o$	$(x, x, 0)$	$\lambda = (1 - b)x^2$	$-2\lambda$ , eigenvalues of $2 \times 2$ matrix with tr = $\mu - 2(1 + b - c)x^2$ det = $-2x^2\{(1 + b)\mu + 2((1 + b)c - e)x^2\}$

Table 1: Branching equations and stability assignments for the primary branches of equilibria.

and are unstable if one or both of these inequalities is reversed.

The  $\mathbb{D}_1^o$  equilibria exist for  $\lambda > 0$  provided  $b < 1$ , in which case they are asymptotically stable if

$$(1 - b)\mu - 2(1 + b - c)\lambda < 0, \quad (b^2 - 1)\mu + 2(e - (1 + b)c)\lambda > 0,$$

and are unstable if one or both of these inequalities is reversed.

## Secondary bifurcations

Next, we describe the secondary bifurcations of equilibria and periodic solutions that bifurcate from the three primary branches of equilibria.

Table 1 gives information on the eigenvalues associated to the three primary branches of equilibria. Secondary bifurcations occur when the real parts of the eigenvalues vanish. Zero eigenvalues signify steady-state bifurcation to secondary branches of equilibria, and imaginary eigenvalues signify Hopf bifurcation to secondary branches of periodic solutions.

**Proposition 2.4** (a) *Secondary branches of equilibria bifurcate from the primary branches of equilibria as follows:*

$\mathbb{Z}_4$     None.

$\mathbb{D}_1^e$     At  $(1 + b)\mu + ((1 + b)c - e)\lambda = 0$ .

$\mathbb{D}_1^o$     At  $(b^2 - 1)\mu + 2(e - (1 + b)c)\lambda = 0$ .

*These secondary bifurcations are pitchfork bifurcations and the bifurcating equilibria have trivial isotropy.*

*(b) Secondary branches of periodic solutions bifurcate from the primary branches of equilibria as follows:*

$$\mathbb{Z}_4 \quad \text{At } \lambda + d\mu = 0.$$

$$\mathbb{D}_1^e \quad \text{At } \mu + (1 + b + c)\lambda = 0 \text{ provided } (1 + b)^2 + e < 0.$$

$$\mathbb{D}_1^v \quad \text{At } (1 - b)\mu - 2(1 + b - c)\lambda = 0 \text{ provided } -(1 + b)^2 + e > 0.$$

*The resulting periodic solutions have trivial spatial symmetry and spatiotemporal symmetry  $\mathbb{Z}_4$ ,  $\mathbb{D}_1^e$ , and  $\mathbb{D}_1^v$  respectively. For example, the  $\mathbb{Z}_4$  branch has quarter-period phase shift symmetry coupled with the action of  $\rho$ .*

**Proof** The eigenvalues for  $\mathbb{Z}_4$  are given explicitly in Table 1, so the secondary bifurcations are immediate. The results for  $\mathbb{D}_1^e$  and  $\mathbb{D}_1^v$  are obtained by noting that for a  $2 \times 2$  matrix, zero eigenvalues are signified by  $\det A = 0$  and imaginary eigenvalues are signified by  $\text{tr } A = 0$ ,  $\det A > 0$ .

Finally, the results on spatiotemporal symmetry are a consequence of the equivariant Hopf theorem [16]. ■

It follows from general principles that the secondary branches of equilibria and periodic solutions in Proposition 2.4 satisfy “exchange of stability”, so their stability is governed by the stability of the primary branch together with the branching direction. Computing the direction of branching is elementary but tedious. We focus on asymptotically stable periodic solutions bifurcating from the  $\mathbb{Z}_4$  and  $\mathbb{D}_1^e$  branches.

**Lemma 2.5** *If  $b + 4cd < 3$ , then the  $\mathbb{Z}_4$  periodic solutions bifurcate supercritically (for  $\lambda + d\mu > 0$ ) and are asymptotically stable. If*

$$(1 + b)^2 + e < 0, \text{ and } (1 + b)(2b^3 + 3b^2 - 3b + 2be + 3bc + 2ce + 2b^2c) > 0,$$

*then the  $\mathbb{D}_1^e$  periodic solutions bifurcate supercritically (for  $\mu + (1 + b + c)\lambda > 0$ ) and are asymptotically stable.*

*If the appropriate inequality is reversed, then the corresponding periodic solutions exist subcritically and are unstable.*

The proof is given in an appendix.

### 3 Tertiary bifurcations

To compute the loss of stability of the secondary branches of periodic solutions, and the corresponding onset of symmetric chaos, it is necessary to use numerical methods. From now on, we specify the values of the constants  $b, c, d, e$  in the vector field (2.1) as follows:

$$b = 0.9 \quad c = -2.1 \quad d = -0.05 \quad e = -19.2$$

We concentrate on the positive quadrant  $\lambda, \mu > 0$  of parameter space. Applying the results of Section 2 with these values, we find that the primary branches of equilibria with  $\mathbb{Z}_4$  and  $\mathbb{D}_1^e$  symmetry are initially asymptotically stable, and each undergo supercritical Hopf bifurcation to secondary branches of periodic solutions with spatiotemporal  $\mathbb{Z}_4$  and  $\mathbb{D}_1^e$  symmetry. The Hopf bifurcations occur at  $\mu = 20\lambda$  and  $\mu = 0.2\lambda$  respectively. Primary branches of  $\mathbb{D}_1^v$  equilibria exist but are unstable.

In this section, we use AUTO and DsTool to study the dynamics that occurs when the secondary branches of  $\mathbb{Z}_4$  and  $\mathbb{D}_1^e$  symmetric periodic solutions lose stability.

#### Loss of stability of the secondary periodic solutions

In this subsection, we use AUTO [12] to determine curves in  $\lambda$ - $\mu$  parameter space where tertiary bifurcations take place from the secondary branches of periodic solutions. At the same time, we determine the manner in which the periodic solutions lose stability.

The use of AUTO is slightly nonstandard due to the spatiotemporal symmetry of the periodic solutions. Standard implementation of AUTO leads to bifurcations that AUTO cannot recognise, and so the approach must be modified as described below.

**$\mathbb{Z}_4$  periodic solutions** The  $\mathbb{Z}_4$  periodic solutions have spatiotemporal symmetry

$$(x, y, w)(t + T/4) = \rho \cdot (x, y, w)(t) = (-y, x, w)(t),$$

where  $T$  is the period of the periodic solution.

Solutions with this symmetry type can be computed numerically by constructing a modified Poincaré map  $P$ . Let  $X$  be a local two-dimensional cross-section (we chose  $X$  contained in the plane  $\{w = c\}$  for some constant  $c$ ). Let  $g : X \rightarrow \rho X$  be the first hit map and define  $P = \rho^{-1}g : X \rightarrow X$ . Then periodic solutions with  $\mathbb{Z}_4$  spatiotemporal symmetry correspond to fixed points of  $P$ . Working with  $P$  is more efficient numerically than working with the usual Poincaré map since it is sufficient to compute only one quarter of the solution. More significantly, the bifurcations for  $P$  are the generic ones, see Remark 3.1 below.



To compute the solutions, we used AUTO to find fixed points of  $P$ , starting with a solution near to the Hopf bifurcation point. By increasing  $\lambda$ , a path of periodic solutions was computed and it was found that the solutions on this path lost stability at a turning point. Two parameter continuation was used to follow the path of turning points in the two parameter  $(\lambda, \mu)$  space, shown in Figure 2.

$\mathbb{D}_1^e$  **periodic solutions** The  $\mathbb{D}_1^e$  periodic solutions have spatiotemporal symmetry

$$(x, y, w)(t + T/2) = \kappa \cdot (x, y, w)(t) = (x, -y, -w)(t).$$

We again consider a local cross-section  $X$  ( $\{w = c\}$  suffices) and let  $g : X \rightarrow \kappa X$  denote the first hit map. Periodic solutions with  $\mathbb{D}_1^e$  symmetry correspond to fixed points for the modified Poincaré map  $P = \kappa g : X \rightarrow X$ .

Using AUTO, we found that the path of stable fixed points for  $P$  loses stability via a period-doubling bifurcation. For the underlying flow, this corresponds to a symmetry-breaking pitchfork bifurcation to nonsymmetric periodic solutions. The path of bifurcations is shown in the  $(\lambda, \mu)$  plane in Figure 2.

**Remark 3.1** We note that this is not a period-doubling bifurcation for the flow and is an example of “suppression of period-doubling” [26]. In fact, the bifurcating nonsymmetric periodic solutions are approximately of the same period as the  $\mathbb{D}_1^e$  periodic solutions near the bifurcation point.

If we had ignored the spatiotemporal symmetry, then the ordinary Poincaré map obtained by integrating around the full periodic solution would have an eigenvalue 1 at the bifurcation point, but the bifurcation is a pitchfork rather than a turning point. This is a highly degenerate bifurcation in systems without symmetry and is not recognised by AUTO.

The pitchfork bifurcation to nonsymmetric periodic solutions turns out to be subcritical, resulting in unstable solutions initially. However, there is almost immediately a turning point at which they regain stability. The corresponding hysteretic region of bistability is extremely thin. The turning point is quickly followed by a period-doubling cascade. We computed the first period-doubling bifurcation, and the path of bifurcation points is shown as a dashed curve in Figure 2.

To summarise, Figure 2 shows the paths of Hopf bifurcations from primary equilibria to secondary periodic solutions (solid straight lines), and the paths of initial loss of stability of the secondary periodic solutions (solid curves). The thin hysteretic region where stable  $\mathbb{D}_1^e$ -periodic solutions and asymmetric periodic solutions coexist is not shown (the curve of turning points where the asymmetric periodic solutions gain stability is omitted), but the dashed curve shows the path of first period-doubling bifurcations for the asymmetric periodic solutions.

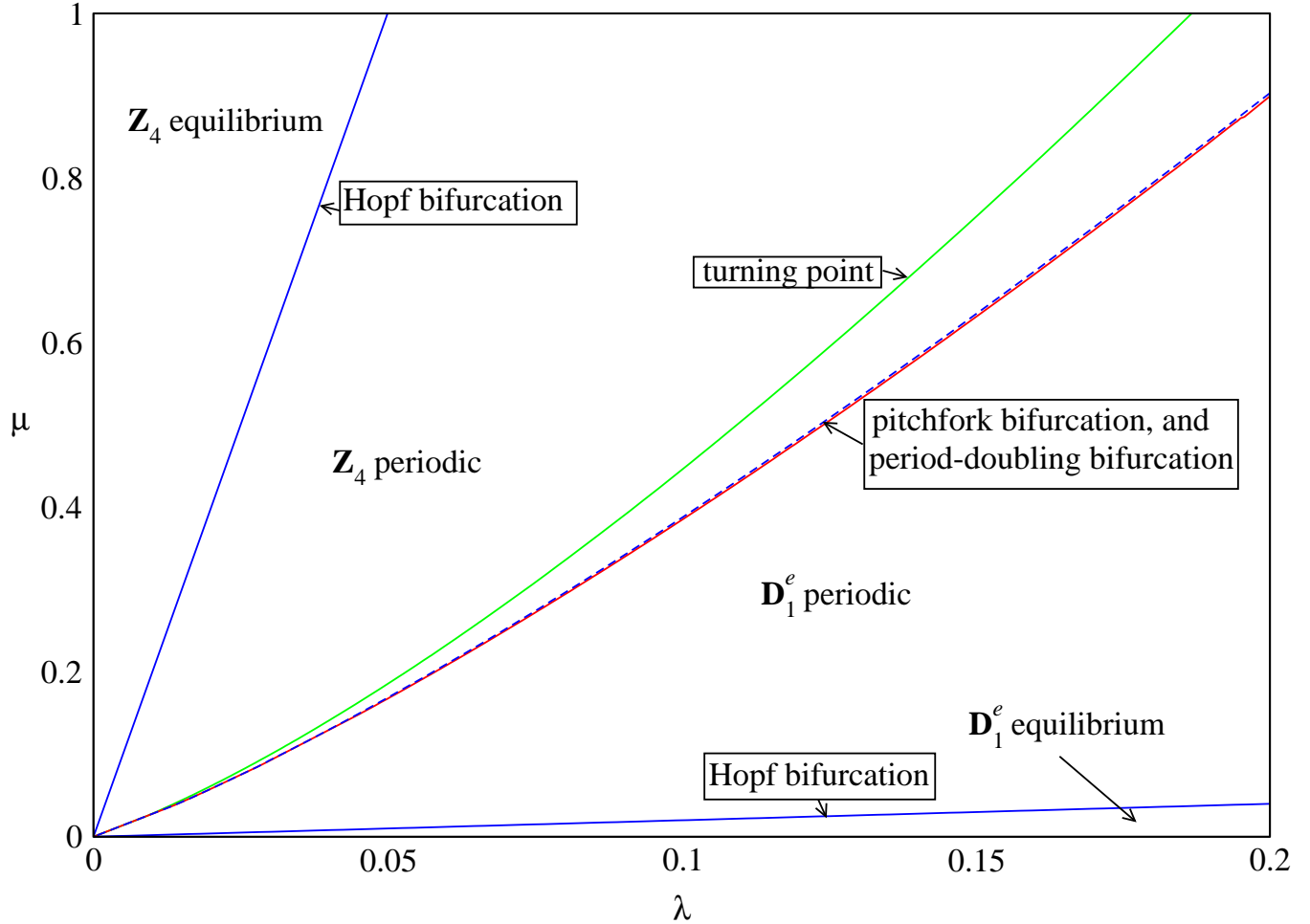


Figure 2: Secondary and tertiary transitions for the vector field (2.1) with  $b = 0.9$ ,  $c = -2.1$ ,  $d = -0.05$ ,  $e = -19.2$ .

### Chaotic transitions

In this subsection, we explore the nature of the tertiary transitions using DsTool [3]. Throughout, we fix  $\lambda = .16$  and vary  $\mu$ .

Periodic solutions with spatiotemporal symmetry  $\mathbb{D}_1^e$  and  $\mathbb{Z}_4$  are shown in Figures 6 and 7. The parameter values are  $\mu = .68$  and  $\mu = .82$  respectively.

The turning point loss of stability for the  $\mathbb{Z}_4$  periodic solutions takes place near  $\mu = .8186$ . Experiments with DsTool indicate that at the turning point there is a nonhysteretic transition to a  $\mathbb{D}_4$  symmetric chaotic attractor which persists until near  $\mu = .739$ . After this point, there is a collapse to a  $\mathbb{D}_1^e$  symmetric chaotic attractor. Varying  $\mu$  in the other direction, it can be seen that this is a symmetry-increasing

bifurcation from  $\mathbb{D}_1^y$  to  $\mathbb{D}_4$  symmetric chaos. The  $\mathbb{D}_4$  and  $\mathbb{D}_1^y$  symmetric attractors for  $\mu = .74$  and  $\mu = .73$  are shown in Figures 8 and 10. For contrast, an amalgamation of the  $\mathbb{D}_1^c$  and  $\mathbb{Z}_4$  periodic solutions from Figure 6 and 7, together with their symmetry related images, is shown in Figure 9.

Turning to the  $\mathbb{D}_1^c$  periodic solutions, the subcritical pitchfork bifurcation to unstable nonsymmetric periodic solutions occurs at  $\mu = .6835$ . Asymptotically stable nonsymmetric periodic solutions exist for  $.6821 \leq \mu \leq .6869$  with a period-doubling bifurcation at  $\mu = .6869$ . Experiments with DsTool indicate that a sequence of period-doubling bifurcations follows, leading to a nonsymmetric chaotic attractor at around  $\mu = .688$ . There is then a symmetry-increasing bifurcation at around  $\mu = .6891$  to a fully  $\mathbb{D}_4$  symmetric chaotic attractor.

The ensuing region of parameter space seems to be extremely complicated with numerous transitions between periodic/chaotic solutions with/without  $\mathbb{D}_1^y$  symmetry. The transitions take the form of period-doubling sequences, gluing bifurcations and symmetry-increasing bifurcations. Periodic solutions with no symmetry and with  $\mathbb{D}_1^y$  symmetry are shown in Figure 11.

Eventually, a region of parameter space is reached ( $.720 \leq \mu \leq .738$ ) where  $\mathbb{D}_1^y$  symmetric chaotic attractors appear to dominate. This region terminates in the afore-mentioned symmetry-increasing bifurcation to the  $\mathbb{D}_4$  symmetric attractor.

It is not entirely clear from Figure 8 that the chaotic attractor at  $\lambda = 0.16$ ,  $\mu = 0.74$  is fully  $\mathbb{D}_4$ -symmetric as claimed. In fact, it is hard to plot a trajectory of sufficient length to resolve this issue. (There are 200,000 data points, but our time step is 0.01 so the total integration time is only 2000 time units.) In Figure 12, we show the same attractor but now in terms of pixels hit by the trajectory. There is no longer a data-storage difficulty, and we use 100,000,000 data points (corresponding to a total integration time of 1,000,000 time units). The symmetries are now clear. Also, in Figure 13, we colour the pixels according to how often the pixel is hit. This gives an idea of the density function for the invariant measure.

## 4 Lyapunov exponents

Our analytic calculations, and the computations using AUTO, leave a large region of parameter space unexplored. The simulations using DsTool indicate that there are chaotic attractors throughout much of this region. To confirm this we computed the maximal Lyapunov exponent for a fixed initial condition (chosen arbitrarily to be  $(x, y, w) = (0.008, 0.044, 0.005)$ ) and a grid of values of  $\lambda$  and  $\mu$ . Our results are shown in Figure 3.

Most of Figure 3 was obtained by varying  $\lambda$  from 0 to 0.2 in increments of 0.002, and varying  $\mu$  from 0 to 1 in increments of 0.01. To obtain greater resolution near

the origin, in the range  $0 \leq \lambda \leq 0.042$ , we used finer increments of 0.002 for  $\mu$ .

For each point in the  $(\lambda, \mu)$  grid, we allowed a transient of 20,000 time units and then computed the maximal Lyapunov exponent over the next 10,000 time units, using a time step of 0.01. There was a clear cutoff between “positive” and “zero” values of the Lyapunov exponent, with the value 0.001 sufficing for our purposes. For example, fixing  $\lambda = 0.1$  and letting  $\mu$  vary from 0.38 to 0.45 in increments of 0.01 yields the exponents

$$\begin{array}{cccc} 1.47 \times 10^{-4} & 7.17 \times 10^{-2} & 5.85 \times 10^{-4} & 5.86 \times 10^{-2} \\ 7.47 \times 10^{-2} & 9.13 \times 10^{-2} & 1.06 \times 10^{-1} & 2.26 \times 10^{-4} \end{array}$$

clearly indicating 5 chaotic parameter values  $\mu = 0.39, 0.41, 0.42, 0.43, 0.44$ .

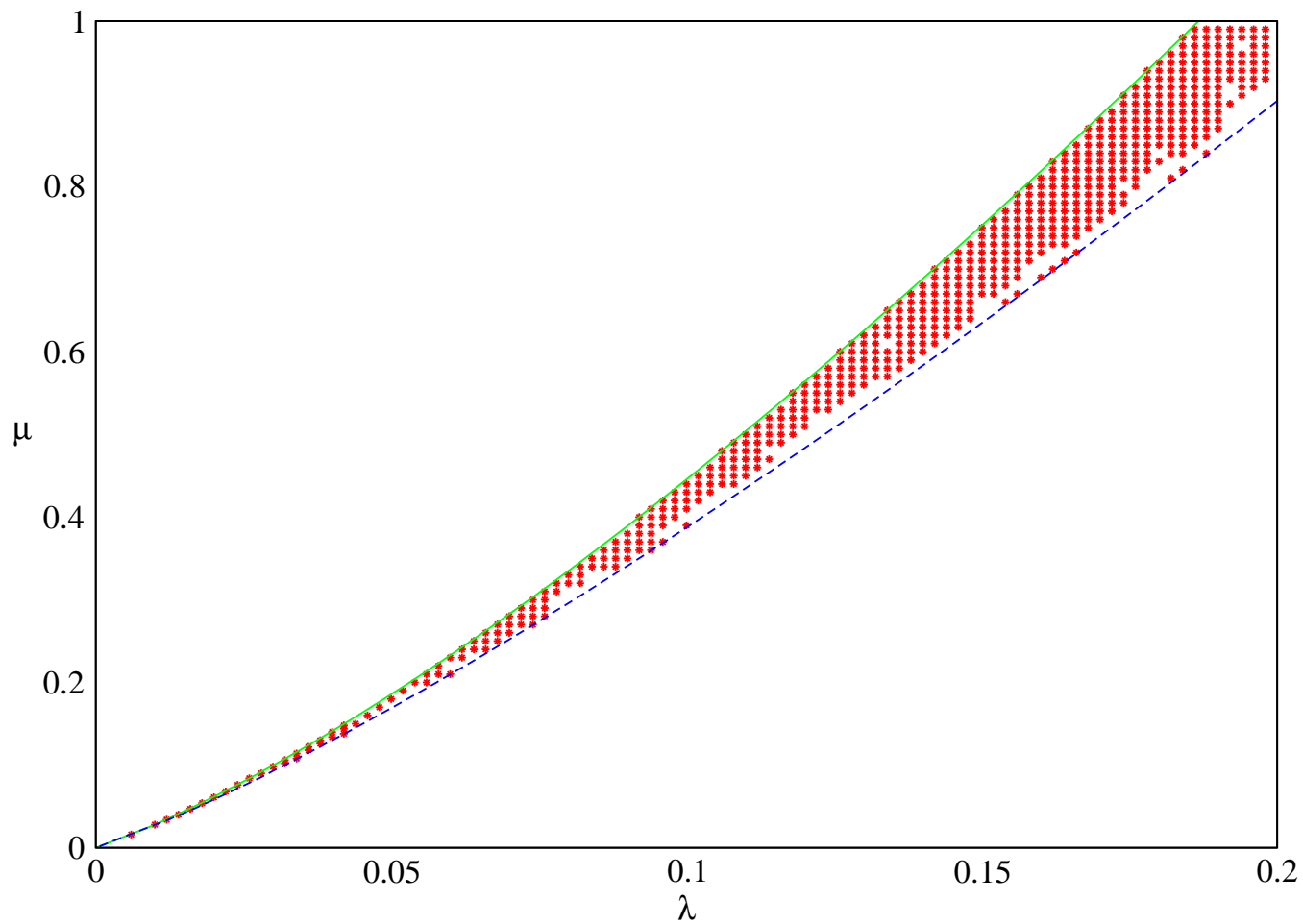


Figure 3: Region of  $(\lambda, \mu)$  parameter space with positive Lyapunov exponent for the vector field (2.1) with  $b = 0.9$ ,  $c = -2.1$ ,  $d = -0.05$ ,  $e = -19.2$ . The boundaries of the regions studied analytically and using AUTO (cf. Figure 2) are also shown.

## 5 Symmetry detectives

Symmetry detectives [4, 10] are a method for numerically computing the symmetry of an attractor. In general, there are two advantages to proceeding in this way:

- (i) For high-dimensional dynamical systems and complicated symmetry groups, it might be hard to determine the symmetries visually.
- (ii) The approach can be automated, and so can deal with a large number of parameter values, producing a detailed map of parameter space.

In principle, it is not hard to determine the symmetry of a chaotic attractor for the three-dimensional vector field (2.1) by looking at the projections into the  $(x, y)$  plane. The detective approach is used here primarily because of advantage (ii).

The problem is to determine numerically the symmetries inside  $\mathbb{D}_4$  that preserve a set  $A$  in  $\mathbb{R}^3$ . As shown in Barany *et al.* [4], this can be done by converting the set  $A$  into a point  $\psi_A$  in some higher-dimensional representation space  $V$  for  $\mathbb{D}_4$ , and then computing the symmetry of the point  $\psi_A$ . The key property of  $V$  is that every subgroup of  $\mathbb{D}_4$  should be an isotropy subgroup for the action of  $\mathbb{D}_4$  on  $V$ .

We take the representation space  $V = \mathbb{R}^5$  with coordinates  $v = (v_1, \dots, v_5)$  where the action of  $\mathbb{D}_4$  is defined by

$$\rho \cdot v = (v_1, -v_2, -v_3, -v_5, v_4), \quad \kappa \cdot v = (-v_1, v_2, -v_3, v_4, -v_5).$$

Note that  $V$  splits up into three distinct nontrivial 1-dimensional representations  $\mathbb{R}\{v_1\}$ ,  $\mathbb{R}\{v_2\}$ ,  $\mathbb{R}\{v_3\}$  and the standard 2-dimensional representation  $\mathbb{R}\{v_4, v_5\}$ .

Up to conjugacy, there are 8 subgroups of  $\mathbb{D}_4$ . Six of these are normal subgroups with fixed-point subspaces in  $V$  given by

$$\begin{aligned} \text{Fix } \mathbb{D}_4 &= \{0\}, & \text{Fix } \mathbb{D}_2^e &= \mathbb{R}\{v_2\}, & \text{Fix } \mathbb{D}_2^v &= \mathbb{R}\{v_3\}, \\ \text{Fix } \mathbb{Z}_4 &= \mathbb{R}\{v_1\}, & \text{Fix } \mathbb{Z}_2 &= \mathbb{R}\{v_1, v_2, v_3\}, & \text{Fix } \mathbf{1} &= V. \end{aligned}$$

The remaining subgroups  $\mathbb{D}_1^e$  and  $\mathbb{D}_1^v$  each have two conjugate copies (conjugated by  $\rho$ ) and the union of fixed point spaces is a pair of planes in each case:

$$\text{Fix } \mathbb{D}_1^e = \mathbb{R}\{v_2, v_4\} \cup \mathbb{R}\{v_2, v_5\}, \quad \text{Fix } \mathbb{D}_1^v = \mathbb{R}\{v_3, v_4 + v_5\} \cup \mathbb{R}\{v_3, v_4 - v_5\}.$$

These fixed point spaces are distinct, so each subgroup of  $\mathbb{D}_4$  is indeed an isotropy subgroup for the action on  $V$ .

Next, we define the *detective*

$$\phi(x, y, w) = (w, xyw, xy, x, y).$$

It is easy to see that  $\phi : \mathbb{R}^3 \rightarrow V$  is  $\mathbb{D}_4$ -equivariant with respect to the given actions of  $\mathbb{D}_4$  on  $\mathbb{R}^3$  and  $V$ . In addition,  $\phi$  is a polynomial map and each component of  $\phi$  is nonzero. Hence  $\phi$  satisfies the hypotheses of [4, Theorem 5.2].

At this point we switch to the numerically more efficient method developed by Dellnitz *et al.* [10]. Given an attractor  $A$  with trajectory  $u(t)$ , we define

$$\psi_A = \lim_{T \rightarrow \infty} \frac{1}{T} \int_0^T \phi(u(t)) dt.$$

It follows from the ergodic theorem that  $\psi_A \in V$  is well-defined for almost every initial condition  $u(0)$ , and the point  $\psi_A$  inherits the symmetry of the set  $A$  (under reasonable but technical hypotheses about the ergodic measures on  $A$ ). Moreover, it follows from the properties of  $\phi$  (being a detective) that typically, the symmetry of  $\psi_A$  is identical to the symmetry of  $A$ .

It remains to compute the distance of  $\psi_A$  from the various fixed-point spaces and hence to determine the symmetry of  $A$ . Of many possible algorithms, we chose

- (i) If  $v_1^2 + v_2^2 + v_3^2 + v_4^2 + v_5^2 = 0$ , then  $\mathbb{D}_4$ .
- (ii) Else, if  $v_2^2 + v_3^2 + v_4^2 + v_5^2 = 0$ , then  $\mathbb{Z}_4$ .
- (iii) Else, if  $v_1^2 + v_3^2 + v_4^2 + v_5^2 = 0$ , then  $\mathbb{D}_2^e$ .
- (iv) Else, if  $v_1^2 + v_2^2 + v_4^2 + v_5^2 = 0$ , then  $\mathbb{D}_2^g$ .
- (v) Else, if  $v_4^2 + v_5^2 = 0$ , then  $\mathbb{Z}_2$ .
- (vi) Else, if  $v_1^2 > 0$ , then  $\mathbf{1}$ .
- (vii) Else, if  $v_3^2 > 0$ , then  $\mathbb{D}_1^g$ .
- (viii) Else,  $\mathbb{D}_1^e$ .

(In practice, we have to choose the range of values that numerically constitutes zero.)

Our results are shown in Figure 4. These are based on the same initial conditions for  $(x, y, w)$  and the same values of  $(\lambda, \mu)$  in parameter space that were used in computing Lyapunov exponents in Figure 3. Again, we used time step 0.01 and transient 20,000 time units, but we integrate for the longer time of 100,000 time units. This is necessary to distinguish  $\mathbb{D}_4$  chaotic attractors from  $\mathbb{D}_1^g$  chaotic attractors near the symmetry-increasing bifurcations. In numerical simulations, the chaos is seen immediately, but it sometimes takes longer to see the fully symmetric attractor.

In Figure 5, we show a blown-up version of part of Figure 4.

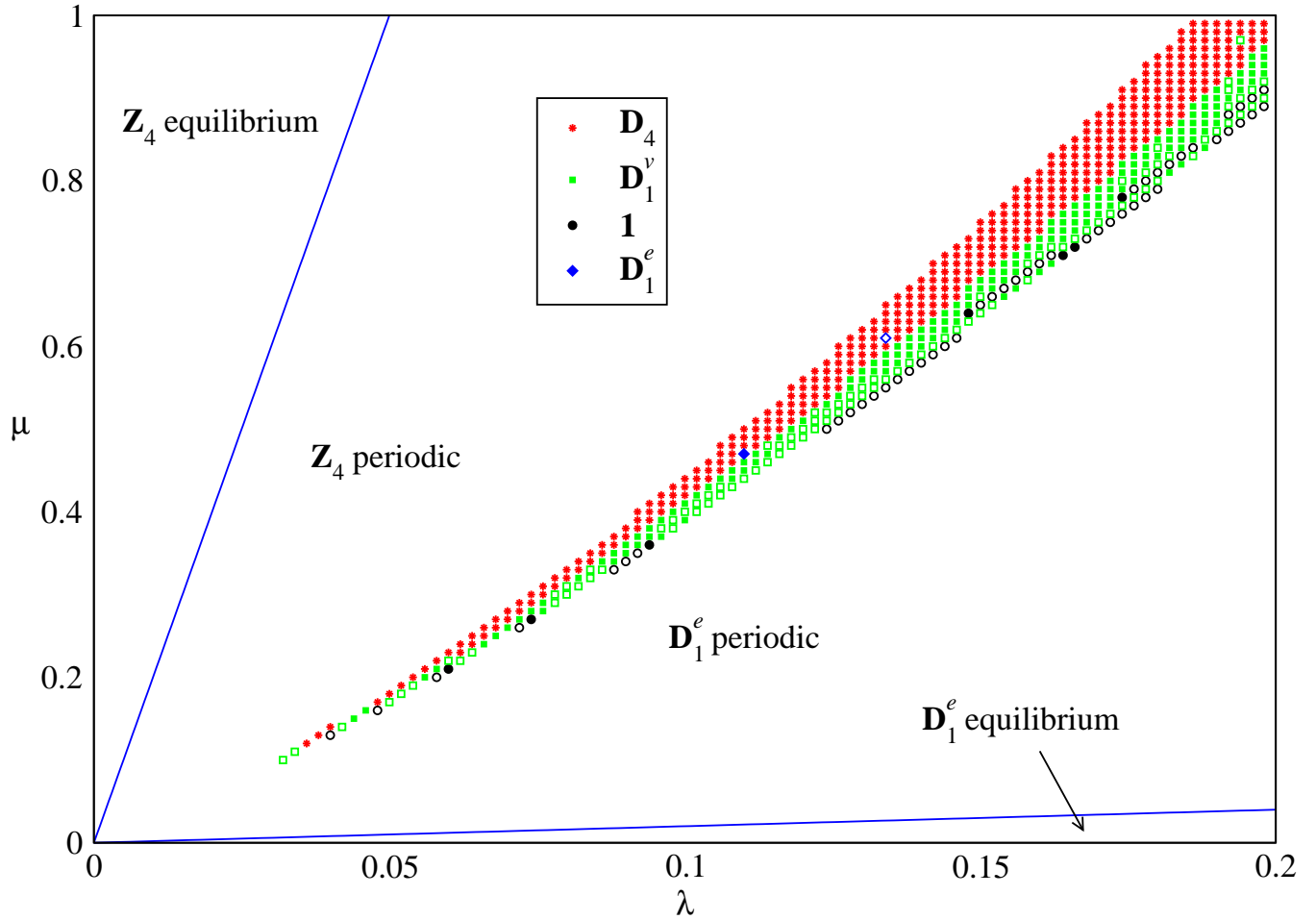


Figure 4: Symmetry types of attractors in  $(\lambda, \mu)$  parameter space for the vector field (2.1) with  $b = 0.9$ ,  $c = -2.1$ ,  $d = -0.05$ ,  $e = -19.2$ . Solid symbols denote chaotic, clear denote nonchaotic. (The  $\mathbb{D}_4$  symmetric attractors are all chaotic.)



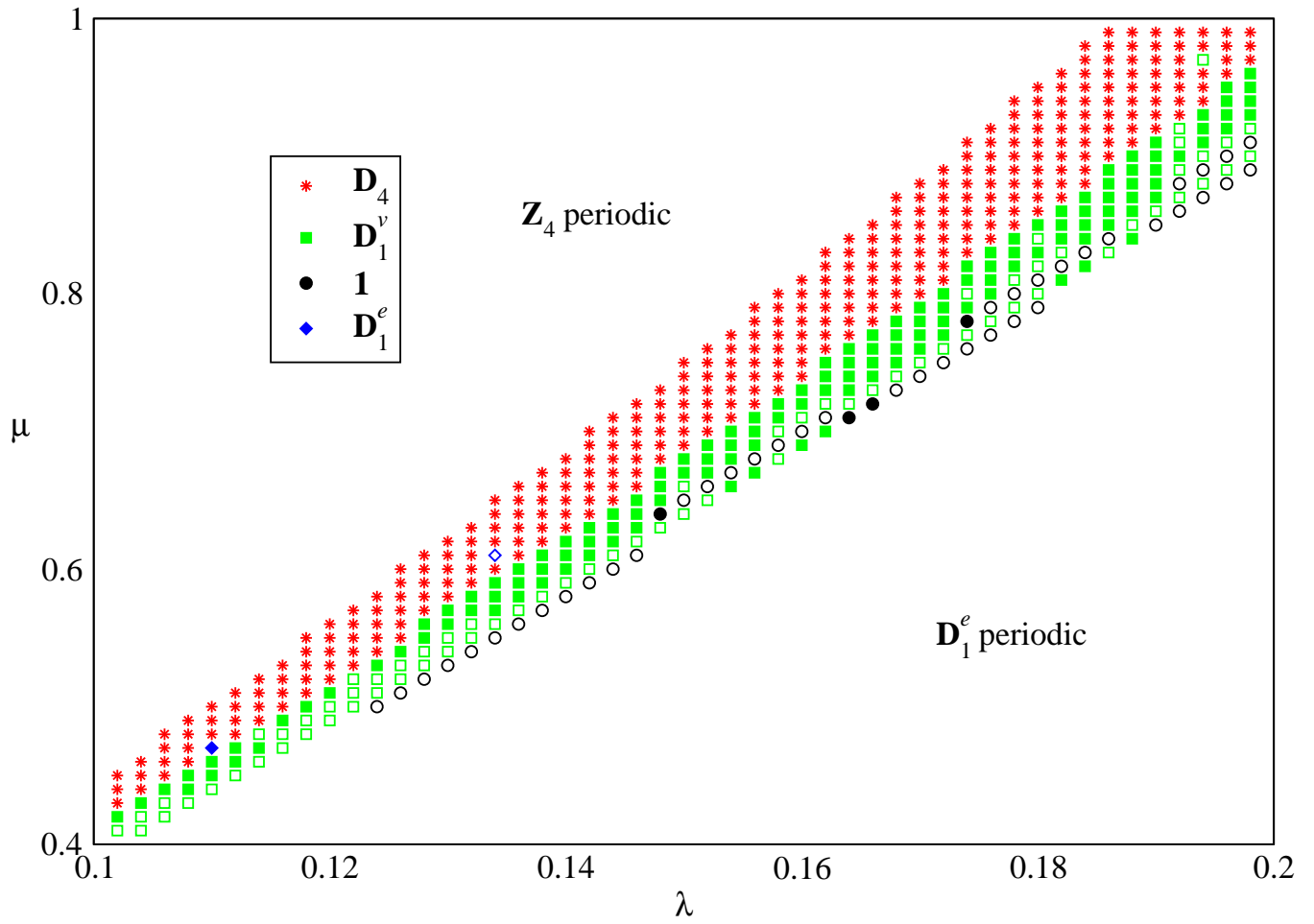


Figure 5: Blow up of subregion of parameter space in Figure 4.

## 6 Conclusions and future directions

In this paper, we have studied a simple-looking codimension two mode interaction with  $\mathbb{D}_4$  symmetry. The codimension two point is the coalescence of two steady-state bifurcation points, and the centre-manifold is three-dimensional.

We computed analytically primary branches of equilibria with maximal isotropy giving rise through Hopf bifurcation to secondary branches of periodic solutions with spatiotemporal symmetry.

Surprisingly, we found tertiary bifurcations to symmetric chaos. Using AUTO, DsTool, Lyapunov exponents, and symmetry detectives, we obtained convincing numerical evidence that the symmetric chaos is part of the local bifurcation, as is various symmetry-increasing bifurcations between chaotic attractors of differing symmetry types.

There are three natural directions that are worthy of further study:

- The corresponding bifurcations with  $\mathbb{D}_n$  symmetry for  $n \neq 4$  are only partially studied. From now on, we write  $\mathbb{D}_1$  as shorthand for  $\mathbb{D}_1^o$  and  $\mathbb{D}_1^e$  when  $n$  is even, and for the unique subgroup of order two (up to conjugacy) when  $n$  is odd. The primary branches of equilibria with  $\mathbb{Z}_n$  and  $\mathbb{D}_1$  symmetry are essentially unchanged and there is still a Hopf bifurcation to a secondary branch of periodic solutions with  $\mathbb{Z}_n$  spatiotemporal symmetry. However, a calculation for  $n \geq 5$  shows that generically the  $\mathbb{D}_1$  equilibria loses stability only via a steady-state bifurcation, hence producing a secondary branch of asymmetric equilibria. In general, the cases  $n \geq 5$  are likely to be simpler than the case  $n = 4$  studied in this paper, since various important terms are now at higher order. The case  $n = 3$  is potentially even more complicated than  $n = 4$  since there are now additional terms at cubic order.

We have not carried out the numerical simulations required to determine the existence of large-scale symmetric chaos and symmetry-increasing bifurcations when  $n = 3$  and  $n \geq 5$ .

- It should be straightforward to write down a system of reaction-diffusion equations in a square domain undergoing the steady-state/steady-state mode interaction studied in this paper. Hence, it should be possible to realise symmetric chaos and symmetry-increasing bifurcations in a local bifurcation in a system of partial differential equations.
- One implication of our investigations is that symmetric chaos should be more common near onset in real experiments than might previously have been anticipated. Likely situations include transitions from a square symmetric equilibrium

in an experiment in a square domain, but also transitions from a four-fold symmetric equilibrium in an experiment in a circular domain (for example, cellular flames in a circular burner). In the situation of a circular domain, the total dynamics would consist of a rotational drift superimposed on the dynamics described in this paper.

## Appendix. Direction of branching for secondary branches of periodic solutions

In this Appendix, we give the proof of Lemma 2.5 which establishes the conditions under which the secondary branches of periodic solutions bifurcate supercritically, and hence are asymptotically stable.

**Direction of branching for  $\mathbb{Z}_4$  periodic solutions** Setting  $\nu = \lambda + d\mu$ ,  $\hat{w} = w - \sqrt{\mu}$ , and dropping the hat's, we obtain

$$\begin{aligned}\dot{x} &= [\nu - x^2 + by^2 + 2d\sqrt{\mu}w + dw^2]x - (\sqrt{\mu} + w)y \\ \dot{y} &= [\nu - y^2 + bx^2 + 2d\sqrt{\mu}w + dw^2]y + (\sqrt{\mu} + w)x \\ \dot{w} &= (c(x^2 + y^2) - 2\sqrt{\mu}w - w^2)(\sqrt{\mu} + w) + exy(x^2 - y^2).\end{aligned}$$

To obtain the centre manifold for the secondary bifurcation, write  $w = h(x, y)$  where  $h$  is at least quadratic. In fact,  $h$  is  $\mathbb{Z}_4$ -invariant, so  $w = \alpha(x^2 + y^2) + \dots$  where we have neglected terms of order 4 or higher. A calculation shows that  $\alpha = \frac{c}{2\sqrt{\mu}} + \dots$  and the centre manifold equations are given by

$$\begin{aligned}\dot{x} &= [\nu + (cd - 1)x^2 + (b + cd)y^2 + \dots]x - (\sqrt{\mu} + \dots)y \\ \dot{y} &= [\nu + (cd - 1)y^2 + (b + cd)x^2 + \dots]y + (\sqrt{\mu} + \dots)x.\end{aligned}$$

Next we put the equation into Birkhoff normal form. Abstractly, we can write the system as

$$\begin{aligned}\dot{x} &= (\nu + \alpha x^2 + \beta y^2)x - \omega y \\ \dot{y} &= (\nu + \alpha y^2 + \beta x^2)y + \omega x.\end{aligned}$$

Making the near identity  $\mathbb{Z}_4$ -equivariant change of coordinates  $(x, y) = (X + \delta Y^3, Y - \delta X^3)$  yields at lowest order

$$\begin{aligned}\dot{X} &= (\nu + (\alpha + \omega\delta)X^2 + (\beta - 3\omega\delta)Y^2)X - \omega Y \\ \dot{Y} &= (\nu + (\alpha + \omega\delta)Y^2 + (\beta - 3\omega\delta)X^2)Y - \omega X.\end{aligned}$$

Setting  $\delta = (\beta - \alpha)/(4\omega)$  yields

$$\begin{aligned}\dot{X} &= (\nu + C(X^2 + Y^2))X - \omega Y \\ \dot{Y} &= (\nu + C(X^2 + Y^2))Y - \omega X\end{aligned}$$

where  $C = \frac{1}{4}(3\alpha + \beta) = \frac{1}{4}(b + 4cd - 3)$ . Thus supercritical bifurcation corresponds to  $C < 0$  yielding the condition  $b + 4cd < 3$  in Lemma 2.5.

**Direction of branching for  $\mathbb{D}_1^e$  periodic solutions** Setting  $\nu = \mu + (1 + b + c)\lambda$ ,  $\hat{x} = x - \sqrt{\lambda}$  and dropping the hat's, we obtain

$$\begin{aligned}\dot{x} &= (\sqrt{\lambda} + x)(-2\sqrt{\lambda}x - x^2 + by^2 + dw^2) - \omega y \\ \dot{y} &= y((1 + b)\lambda - y^2 + 2b\sqrt{\lambda}x + bx^2 + dw^2) + \sqrt{\lambda}w + \omega x \\ \dot{w} &= w(\nu - (1 + b)\lambda + 2c\sqrt{\lambda}x + cx^2 + cy^2 - w^2) + e(x + \sqrt{\lambda})y(x^2 + 2\sqrt{\lambda}x + \lambda - y^2).\end{aligned}$$

To obtain the centre manifold equations, set  $x = \alpha y^2 + \beta yw + \gamma w^2$ . Plugging this in, and equating coefficients at quadratic order, leaves the following system of linear equations to be solved for  $\alpha, \beta, \gamma$ :

$$2\sqrt{\lambda}\alpha + 2\lambda\beta + 2e\lambda^{3/2}\gamma = -1, \quad 2(2 + b)\sqrt{\lambda}\alpha + e\lambda\beta = b, \quad \sqrt{\lambda}\beta - 2b\lambda\gamma = d\sqrt{\lambda}.$$

We find

$$\begin{aligned}\alpha &= \{2b^2 + 2be - de^2\lambda\}/4\lambda^{1/2}\Delta \\ \beta &= \{-2b(1 + b) + (b + 2)de\lambda\}/2\lambda\Delta \\ \gamma &= \{-2(1 + b) + d(e - 2b - 4)\lambda\}/4\lambda^{3/2}\Delta,\end{aligned}$$

where  $\Delta = b^2 + 2b + e < 0$  (by the hypothesis in Proposition 2.4).

The equations on the centre manifold are given by

$$\begin{aligned}\dot{y} &= (1 + b)\lambda y + \sqrt{\lambda}w + (2\sqrt{\lambda}b\alpha - 1)y^3 + (2\sqrt{\lambda}b\beta + \alpha)y^2w \\ &\quad + (2\sqrt{\lambda}b\gamma + d + \beta)yw^2 + \gamma w^3 \\ \dot{w} &= e\lambda^{3/2}y + (\nu - (1 + b)\lambda)w + e(3\lambda\alpha - \sqrt{\lambda})y^3 + (2c\sqrt{\lambda}\alpha + c + 3e\lambda\beta)y^2w \\ &\quad + (2c\sqrt{\lambda}\beta + 3e\lambda\gamma)yw^2 + (2c\sqrt{\lambda}\gamma - 1)w^3.\end{aligned}$$

Linear algebra plus Birkhoff normal form leads to the normal form equations

$$\dot{z} = \left(\frac{1}{2}\nu + i\omega\right)z + C|z|^2z + \dots$$

Here,  $\omega = \lambda\sqrt{-((1 + b)^2 + e)}$  and  $C = \frac{1}{4}(1 + b)k\lambda/\Delta + O(\lambda^2)$  where

$$k = 2b^3 + 3b^2 - 3b + 2be + 3bc + 2ce + 2b^2c.$$

**Acknowledgements** We are grateful to Marty Golubitsky for several helpful comments and suggestions. The research of SA was supported in part by Fundação para a Ciência e a Tecnologia and Fundo Social Europeu, III Quadro Comunitario de Apoio and by MASIE.

## References

- [1] D. Armbruster, J. Guckenheimer and S. Kim. Chaotic dynamics in systems with square symmetry. *Phys. Lett. A* **140** (1989) 416–420.
- [2] P. Ashwin and I. Melbourne. Symmetry groups of attractors. *Arch. Rational Mech. Anal.* **126** (1994) 59–78.
- [3] A. Back, J. Guckenheimer, M. Myers, F. Wicklin and P. Worfolk. Computer assisted exploration of dynamical systems. *Notices Amer. Math. Soc.* (1992) 303–309.
- [4] E. Barany, M. Dellnitz and M. Golubitsky. Detecting the symmetry of attractors. *Physica D* **67** (1993) 66–87.
- [5] S. B. S. D. Castro. Private communication.
- [6] S. B. S. D. Castro and A. A. du Plessis. Intrinsic transversals. In preparation.
- [7] P. Chossat and M. Golubitsky. Symmetry-increasing bifurcation of chaotic attractors. *Physica D* **32** (1988) 423–436.
- [8] J. H. P. Dawes. A Hopf/steady-state mode interaction in rotating convection: bursts and heteroclinic cycles in a square periodic domain. *Physica D* **149** (2001) 197–209.
- [9] M. Dellnitz, M. Golubitsky and I. Melbourne. Mechanisms of symmetry creation. *Bifurcation and Symmetry* (E. Allgower et al., ed.), ISNM **104**, Birkhäuser, Basel, 1992, pp. 99–109.
- [10] M. Dellnitz, M. Golubitsky and M. Nicol. Symmetry of attractors and the Karhunen-Loève decomposition. *Trends and Perspectives in Applied Mathematics* (L. Sirovich, ed.), Appl. Math. Sci. **100**, Springer, 1994, pp. 73–108.
- [11] M. Dellnitz and C. Heinrich. Admissible symmetry increasing bifurcations. *Nonlinearity* **8** (1995) 1039–1066.

- [12] E. J. Doedel. AUTO, a program for the automatic bifurcation analysis of autonomous systems. *Cong. Numer.* **30** (1981) 265–384.
- [13] M. J. Field. *Lectures on bifurcations, dynamics and symmetry*. Pitman Research Notes in Math. **356**, Addison Wesley Longman Ltd, Harlow, 1996.
- [14] M. J. Field, I. Melbourne and M. Nicol. Symmetric attractors for diffeomorphisms and flows. *Proc. London Math. Soc.* **72** (1996) 657–696.
- [15] M. Golubitsky and D. Schaeffer. *Singularities and Groups in Bifurcation Theory, Vol. I*. Appl. Math. Sci. **51**, Springer, New York, 1985.
- [16] M. Golubitsky, I. N. Stewart and D. Schaeffer. *Singularities and Groups in Bifurcation Theory, Vol. II*. Appl. Math. Sci. **69**, Springer, New York, 1988.
- [17] C. Grebogi, E. Ott, F. Romeiras and J. A. Yorke. Critical exponents for crisis induced intermittency. *Phys. Rev. A* **36** (1987) 5365–5380.
- [18] J. Guckenheimer and P. Holmes. *Nonlinear Oscillations, Dynamical Systems, and Bifurcations of Vector Fields*. Appl. Math. Sci. **42**, Springer, New York, Heidelberg, Berlin, 1990.
- [19] J. Guckenheimer and P. Worfolk. Instant chaos. *Nonlinearity* **5** (1992) 1211–1222.
- [20] M. Higuera, J. Porter and E. Knobloch. Heteroclinic dynamics in the nonlocal parametrically driven nonlinear Schrödinger equation. *Physica D* **162** (2002) 155–187.
- [21] G. P. King and I. N. Stewart. Symmetric chaos. *Nonlinear Equations in the Applied Sciences* (W. F. Ames and C. F. Rogers, eds.), Academic Press, 1991, pp. 257–315.
- [22] A. Lari-Lavassani, W. F. Langford, K. Huseyin and K. Gatermann. Steady-state mode interactions for  $D_3$  and  $D_4$ -symmetric systems. *Dynam. Contin. Discrete Impuls. Systems* **6** (1999) 169–209.
- [23] I. Melbourne, M. Dellnitz and M. Golubitsky. Structure of symmetric attractors. *Arch. Rational Mech. Anal.* **123** (1993) 75–98.
- [24] J. Porter and E. Knobloch. Complex dynamics in the 1:3 spatial resonance. *Physica D* **143** (2000) 138–168.
- [25] A. M. Rucklidge. Global bifurcations in the Takens-Bogdanov normal form with  $D_4$  symmetry near the  $O(2)$  limit. *Phys. Lett. A* **284** (2001) 99–111.

- [26] J. W. Swift and K. Wiesenfeld. Suppression of period doubling in symmetric systems. *Phys. Rev. Lett.* **52** (1984) 705–708.

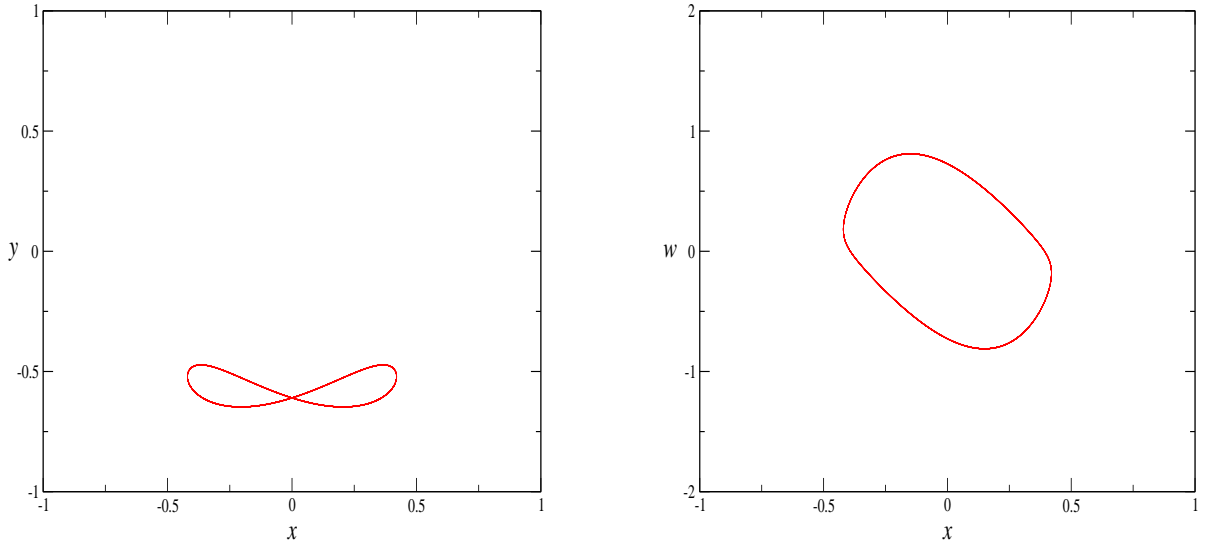


Figure 6: Projection into the  $(x, y)$ - and  $(x, w)$ -planes of the  $\mathbb{D}_1^c$  symmetric periodic solution at  $\lambda = 0.16$ ,  $\mu = 0.68$ . The plot includes 7,000 data points gathered with time step 0.01.

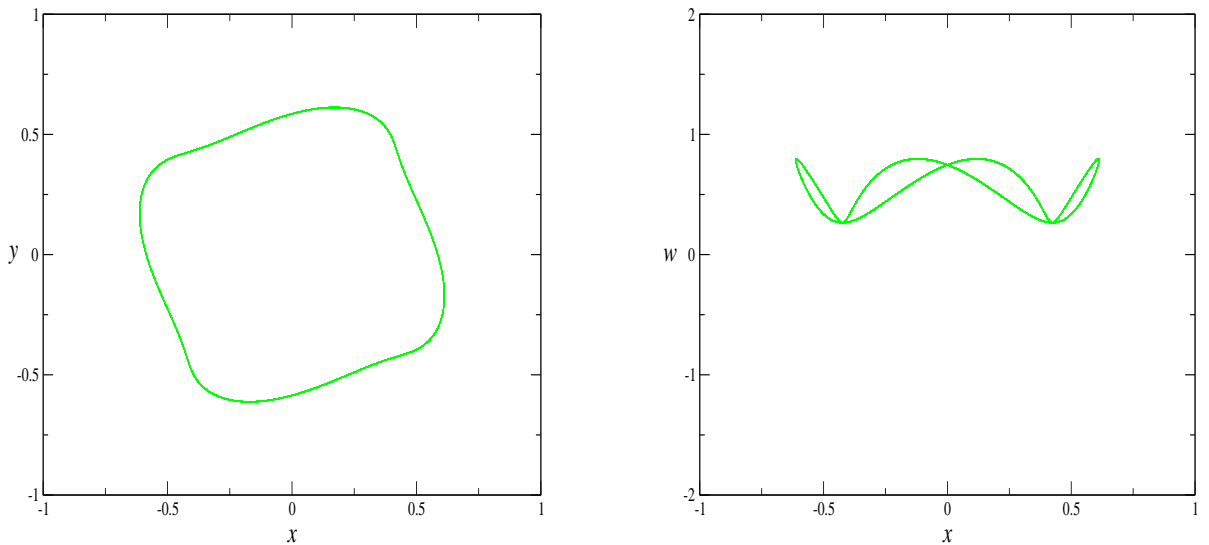


Figure 7: Projection into the  $(x, y)$ - and  $(x, w)$ -planes of the  $\mathbb{Z}_4$  symmetric periodic solution at  $\lambda = 0.16$ ,  $\mu = 0.82$ . The plot includes 7,000 data points gathered with time step 0.01.



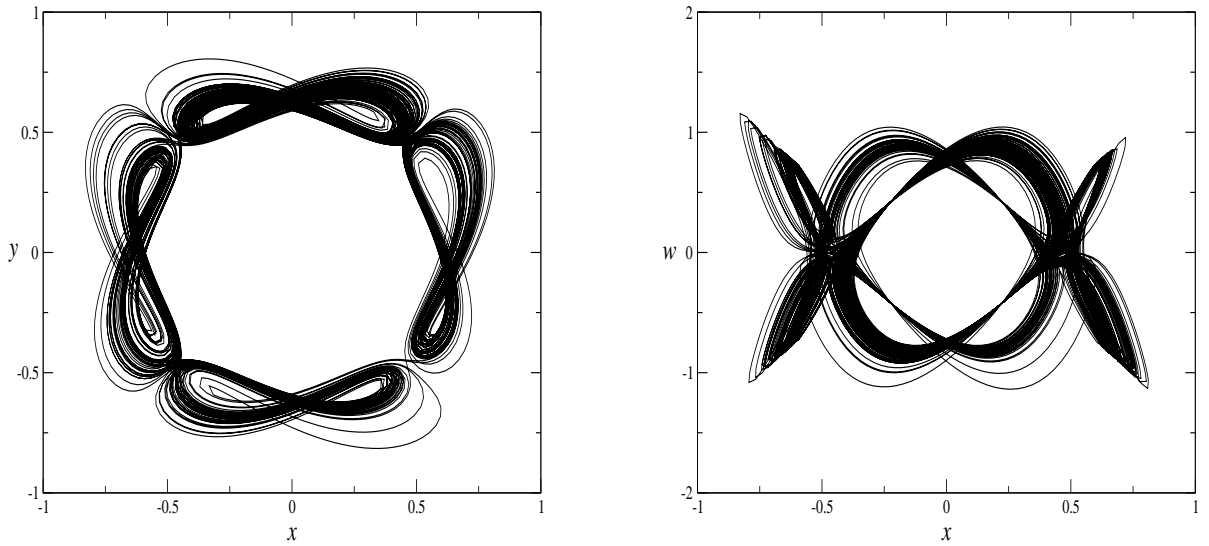


Figure 8: Projection into the  $(x, y)$ - and  $(x, w)$ -planes of the  $\mathbb{D}_4$  symmetric attractor at  $\lambda = 0.16$ ,  $\mu = 0.74$ . The plot includes 200,000 data points gathered with time step 0.01.

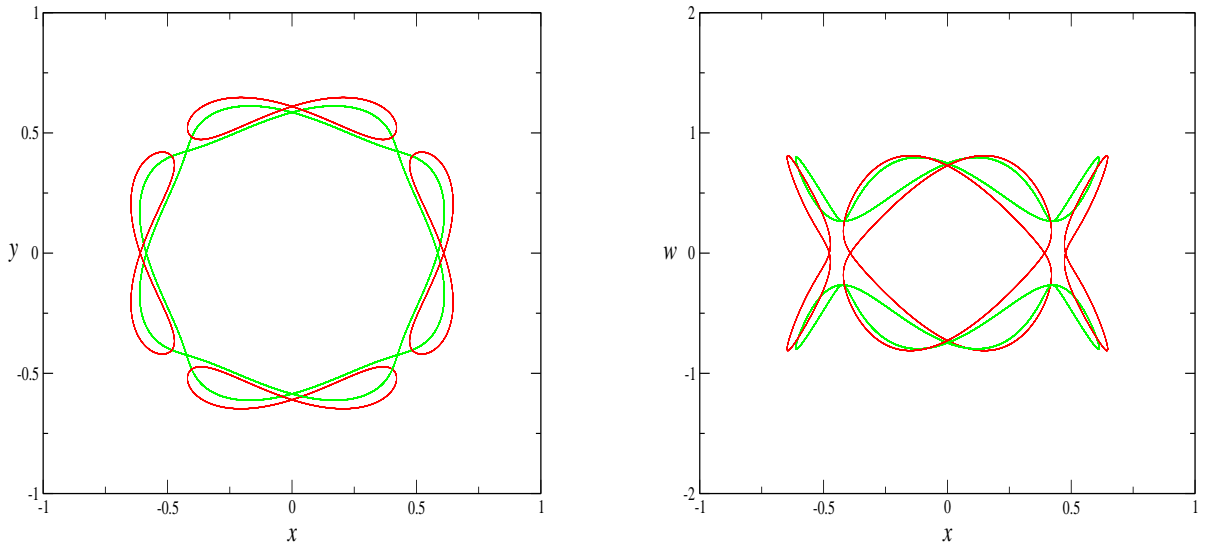


Figure 9: Amalgamation of the plots of the the  $\mathbb{Z}_4$  symmetric and  $\mathbb{D}_1^e$  symmetric periodic solutions shown in Figures 6 and 7, together with their symmetric images.

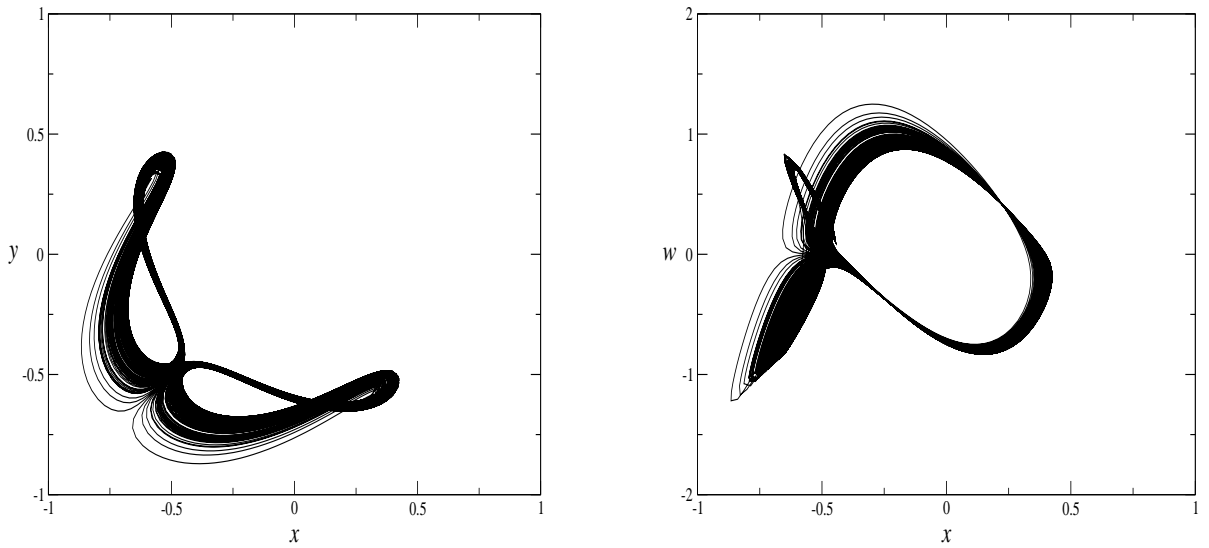


Figure 10: Projection into the  $(x, y)$ - and  $(x, w)$ -planes of the  $\mathbb{D}_1^v$  symmetric attractor at  $\lambda = 0.16$ ,  $\mu = 0.73$ . The plot includes 200,000 data points gathered with time step 0.01.

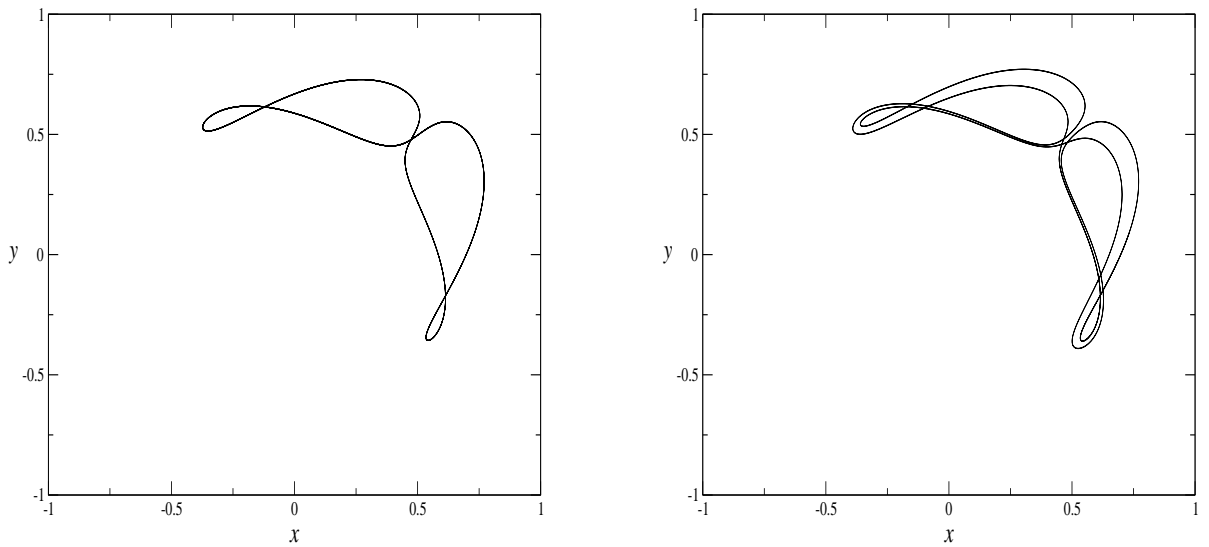


Figure 11: Projection into the  $(x, y)$ -plane of the asymmetric and  $\mathbb{D}_1^v$  symmetric periodic solutions at  $\lambda = 0.16$ ,  $\mu = 0.70$  and at  $\lambda = 0.16$ ,  $\mu = 0.71$ . Each plot includes 7,000 data points.